npj | climate and atmospheric science

www.nature.com/npjclimatsci

ARTICLE OPEN

Check for updates

Differential expansion speeds of Indo-Pacific warm pool and deep convection favoring pool under greenhouse warming

Jeremy Cheuk-Hin Leung[1], Banglin Zhang[1,2,3]✉, Qiuying Gan[1,4], Lei Wang[4], Weihong Qian[1,5] and Zeng-Zhen Hu[6]

The Indo-Pacific warm pool (IPWP), which affects the global climate system through supporting tropical convection, has been reported to expand significantly under greenhouse warming. Although early research revealed that the sea surface temperature (SST) threshold for deep convection (σ_{conv}) increases with global warming, many latest relevant works were still conducted based on the traditional IPWP definition (e.g., static SST = 28 °C threshold, and is referred to as the oceanic warm pool, OWP_{28}). Here, we claim that the OWP_{28} expansion differs from the deep convection favoring pool (DCFP) area change and may not reflect the direct impacts of Indo-Pacific warming on the climate system. Results show that, because of the long-term increase in σ_{conv}, the DCFP expands at a rate 2.6 times slower than the OWP_{28} from 1979 to 2020. The difference reaches 12–27 times from 2015–2100 under different emission scenarios, based on CMIP6 model simulations. While the OWP_{28} expands to the eastern Pacific, the DCFP will remain within the Indian Ocean and western Pacific Ocean regardless of emission levels. This study emphasizes the necessity of considering the response of the relationship between deep convection and SST to climate change when studying the long-term variability of the IPWP.

npj Climate and Atmospheric Science (2022)5:97 ; https://doi.org/10.1038/s41612-022-00315-w

INTRODUCTION

The Indo-Pacific warm pool (IPWP), the warmest tropical ocean region located in the western Pacific Ocean and the eastern Indian Ocean, acts as the atmospheric heat and moisture sources influencing the global climate system through consistently supporting and maintaining tropical deep convection throughout the year, and its long-term change is an important signal indicating how greenhouse warming affects the Earth's climate[1–3]. The convections over the IPWP act as the upward branches of both the Hadley and Walker circulations, which determines the global-scale precipitation pattern[4,5]. It also plays a critical role in affecting tropical cyclones activity[6–8], the Madden-Julian Oscillation[4,9], the El Niño Southern Oscillation[5,10,11], Asian-Australian monsoon variability[12–14], and teleconnections to mid-high latitudes[15,16], etc. Because of the IPWP's importance to the global climate system, changes in the IPWP area have implications for the climate response to greenhouse warming. Researchers have been paying close attention to the changes in the IPWP size in recent decades, and it was reported that the IPWP size has been expanding significantly in the past century as the global sea surface temperature (SST) increases under anthropogenic greenhouse warming[1,9,17–19]. For example, Hoyos and Webster (2012) reported that the observed global oceanic warm pool expanded from about $4.0–7.0 \times 10^7$ km^2 during 1920–2000, and the climate model-projected warm pool area increases by 2100 were greater than 70% and 90% relatively to the 2000–2004, under the IPCC A1B and A2 scenario, respectively[18]. Meanwhile, one of the latest published research revealed that the IPWP size was doubled during 1981–2018, in comparison to 1900–1980[9].

In many early studies about the impacts of IPWP expansion on climate systems, the IPWP is considered as the oceanic region that favors atmospheric deep convection and is identified as the region with SST exceeding a certain threshold (usually between 27.5 and 29.0 °C, and mostly 28 °C), a pre-condition that is necessary to favor tropical deep convection[1,3,9]. In the following discussion, we refer the region covered with 28 °C SST to as the oceanic warm pool (OWP_{28})[18]. However, numerous independent works argued that the SST threshold for deep convection (σ_{conv}) has a statistically significant long-term increasing trend in the past few decades, which implies that a higher σ_{conv} is needed to favor deep convection in a warmer climate[18,20–25]. For example, an upward trend in σ_{conv} from 1980 to 2009 was revealed and linked to tropical mean SST in a study published in 2010[20]. Later in 2012, an independent research, based on the relationship between atmospheric column-integrated heating (CIH) and SST, showed that σ_{conv} increased by about 0.5 °C from 1950 to 2004. They also reported that the OWP_{28} expansion overestimates the area change of positive atmospheric heating (or the dynamic warm pool), which was shown to remain constant, based on reanalysis data and the Coupled Model Intercomparison Project phase 3 (CMIP3) simulations[18]. These works suggest that the area change of the 28 °C isotherm may be unequal to the area change of atmospheric convection. Furthermore, under different shared socio-economic pathway (SSP) scenarios, numerical climate models projected that the global average SST will increase by 0.86 °C (SSP1-2.6) to 2.89 °C (SSP5-8.5) from 1995–2014 to 2081–2100[26], which will result in almost the whole tropical ocean being warmer than 28.0 °C by the end of the 21st century under the SSP5-8.5 scenario[17,27]. In such sense, on one hand, according to the traditional IPWP definition, the OWP_{28} would cover most of the tropical-wide ocean; on the other hand, the significant tropical ocean warming also indicates the possibility of a further increase in σ_{conv}[20], implying that some parts of the projected OWP_{28} may not be featured with deep convection activity or even be covered

[1]Guangzhou Institute of Tropical and Marine Meteorology/Guangdong Provincial Key Laboratory of Regional Numerical Weather Prediction, CMA, Guangzhou, China. [2]College of Atmospheric Science, Lanzhou University, Lanzhou, China. [3]Southern Marine Science and Engineering Guangdong Laboratory, Zhuhai, China. [4]Laboratory for Coastal Ocean Variation and Disaster Prediction, College of Ocean and Meteorology, Guangdong Ocean University, Zhanjiang, China. [5]Department of Atmospheric and Oceanic Sciences, Peking University, Beijing, China. [6]Climate Prediction Center, NCEP/NWS/NOAA, 5830 University Research Court, College Park, MD 20740, USA. ✉email: zhangbl@gd121.cn

by atmospheric subsidence, such as the eastern Pacific region[17,18,28]. This disagrees with the definition of the IPWP (or OWP_{28}) which considers constant SST = 28 °C as the threshold for deep convection.

These prior publications suggested a disagreement of the area changes between OWP_{28} and atmospheric convection over the Indo-Pacific Ocean. However, despite some discussion on the variability of σ_{conv} in a global aspect[9,18,20,21,24,25,29], many latest relevant research still stick to the traditional IPWP definition[9,17–19], giving little care to the significance of the changing σ_{conv}. Due to the above reasons, it remains unclear how the changing relationship between SST and deep convection affects the deep convection favoring ocean surface (or deep convection favoring pool, DCFP) over the Indo-Pacific Ocean under greenhouse warming in the past and future, from the view that local SST acts as the heat and moisture sources favoring deep convection thermodynamically. Given the role of IPWP in the global climate system, in terms that deep convection is the key process to transport tropical signals and energy to other parts of the world, it is necessary to consider the variability of SST conditions for deep convection while discussing IPWP expansion. Hence, in this study, using the latest observed data and the state-of-the-art climate model simulations, we aim at exploring the area change of DCFP over the Indo-Pacific Ocean based on the time-varied σ_{conv}, by considering the relationship between deep convection and local SST change. Our results show that although the DCFP tends to expand with global warming, its expansion speed is dramatically slower than that of the OWP_{28} in both past and future climate change, and is more indicative of the deep convection area. The DCFP did not and likely will not expand to a large extent, and will remain within the Indian Ocean and western Pacific Ocean regardless of the anthropogenic emission level in the future climate.

RESULTS

The changing σ_{conv} over the Indo-Pacific Ocean

The variability of σ_{conv} has been revealed by numerous research in regional- and global-scale aspects, especially for the tropical region[18,20,21,29]. In this study, we focus on the σ_{conv} over Indo-Pacific Ocean region (25°S–25°N, 40°E–220°E). The changing σ_{conv} can be estimated by the joint frequency distribution (JFD) of SST and precipitation (P) over the Indo-Pacific Ocean, which reflects the joint probability (i.e., area of grid points) that certain values of SST and P cover (see Methods section). The 42-year average P-SST JFD (Fig. 1a) clearly shows that deep convections, characterized by large monthly precipitation values (e.g., $P \geq 8$ mm/day), over the Indo-Pacific Ocean seldom occur when the SST is below 27.5 °C, and are mostly observed when SST ranges from 27.5–30.0 °C (thin vertical dashed lines in Fig. 1a). This is consistent with the current definition of IPWP, i.e., the region enclosed by the 28 °C isotherm[1]. However, the P-SST JFD exhibits, to first order, a horizontal shift to warmer SST from 1979–2020 (Fig. 1b). The high joint frequency area of $P \geq 8$ mm/day is originally observed between 27.5–30.0 °C in 1979 (Fig. 1c), but then shifted to 28.0–30.5 °C in 2020 (Fig. 1d). The long-term shift of the P-SST JFD indicates that there is a consistent increase in σ_{conv} over the Indo-Pacific region.

We further examine the annual time series of σ_{conv} over the Indo-Pacific Ocean. The σ_{conv} that favors convection of different intensities are estimated based on the P-SST joint cumulative frequency distribution (JCFD, Fig. 2a–b) for each year (see Methods section), which reflects the probability (shaded areas in Fig. 2) that a certain precipitation rate is observed below a σ_{conv}. For instance, in 1979, there is 20% (purple shading of Fig. 2a) of convection with $P = 10$ mm/day occurs when SST is lower than 28.1 °C; in other words, 80% of convection with $P = 10$ mm/day is observed when SST is higher than 28.1 °C in 1979. As expected, relatively lower SST is enough for supporting weak convection (e.g., $P = 4.0$ mm/day), and higher SST is needed for stronger convection. Based on the P-SST JCFD, we define σ_{conv} as the minimum SST where more than 80% of the area with $P = 10$ mm/day is observed throughout the year. The choice of 80% is made with the assumption that a small proportion of deep convection is not only triggered purely by warm ocean surface but also induced by other atmospheric systems and dynamic factors. The deep convection criterion of $P = 10$ mm/day is chosen based on two facts: (1) it is above the minimum requirement of deep convection ($P = 8$ mm/day), which is shown in Fig. 3 that the σ_{conv} almost remains unchanged for $P \geq 8$ mm/day but increases with precipitation level for $P < 8$ mm/day; and (2) the σ_{conv} derived from 10 mm/day has an average value (28.2 °C) being consistent with the widely used IPWP definition (28 °C). The choice of $P = 10$ mm/day is partly arbitrary and one could estimate the SST threshold based on other criteria. We have carried out the analyses with different deep convection criteria and found that the conclusions are not sensitive to the choice of deep convection criteria. For more details about the calculation of σ_{conv}, reasons for choosing $P = 10$ mm/day as the deep convection criterion, and the sensitivity test results, readers are referred to the Methods section. In addition, we also define the SST threshold for deep convection based on the changes in the tropical mean SST, which was shown to be a simple but widely used indicator of σ_{conv}[20], for comparisons and mark it as σ_{trop} hereafter.

The estimated σ_{conv} varies year by year, ranging from 27.9 to 28.7 °C during 1979 to 2020, and has an average value of 28.2 °C, being consistent with the current definition of IPWP (Fig. 1e). Time-series analyses show that σ_{conv} has a steady increasing trend with obvious interannual variability. σ_{conv} increases from 28.1 °C in 1979 to 28.7 °C in 2020 (thick vertical dashed lines in Fig. 1c–d and 2a–b), with a long-term linear trend of 0.09 °C/decade (Fig. 1e, statistically significant at the 99.9% confidence level), being consistent with the results of previous research that focus on global or tropical-wide spatial scale analyses[18,20]. Similar increasing trends are also obtained for the SST threshold derived based on different precipitation levels (ranging from 0.09 to 0.10 °C/decade for $P \geq 8$ mm/day; Fig. 1e) and from another SST dataset (Fig. 2c–d and Supplementary Figs. 1–2). It is interesting to note that the σ_{trop} exhibits a slightly larger increasing trend (0.11 °C/decade, significant at the 99.9% confidence level, red line in Fig. 1e) than the σ_{conv} does. This indicates that the increasing rate of tropical mean SST may slightly overestimate the changes in SST threshold for deep convection. The slight difference between the σ_{conv} and σ_{trop} is consistent in both ERSSTv5 and HadISST (Fig. 1e and Supplementary Fig. 1e).

It is also important to note that the relationship between σ_{conv} and precipitation criterion seems not to change under greenhouse warming in the past decades. As shown in Fig. 3, while the curve of σ_{conv} against precipitation slightly shifts upward as a result of the overall increase in σ_{conv} over time, the slope (first derivative) of the curve does not exhibit significant changes in the past four decades. While the past and future greenhouse warming may influence the extremeness of precipitation[30–34], that the σ_{conv} increases with precipitation for $P < 8$ mm/day and stays steady for $P \geq 8$ mm/day implies the consistency of the minimum requirement of deep convection, and hence the validity of the definition of σ_{conv} under the context of climate change.

The above results indicate that warmer Indo-Pacific SST is needed to favor deep convection of the same intensity in the present day compared with the past. This is consistent with numerous previous studies which suggested the strong relationship of tropical upper-tropospheric temperature with convective instability and σ_{conv}. As the upper troposphere warms faster than the lower troposphere does under greenhouse warming, the atmosphere has been stabilized and the enhanced atmospheric instability due to oceanic warming is partly offset[18,20,29]. Consequently, the same SST threshold becomes less favorable for deep convection activity over the

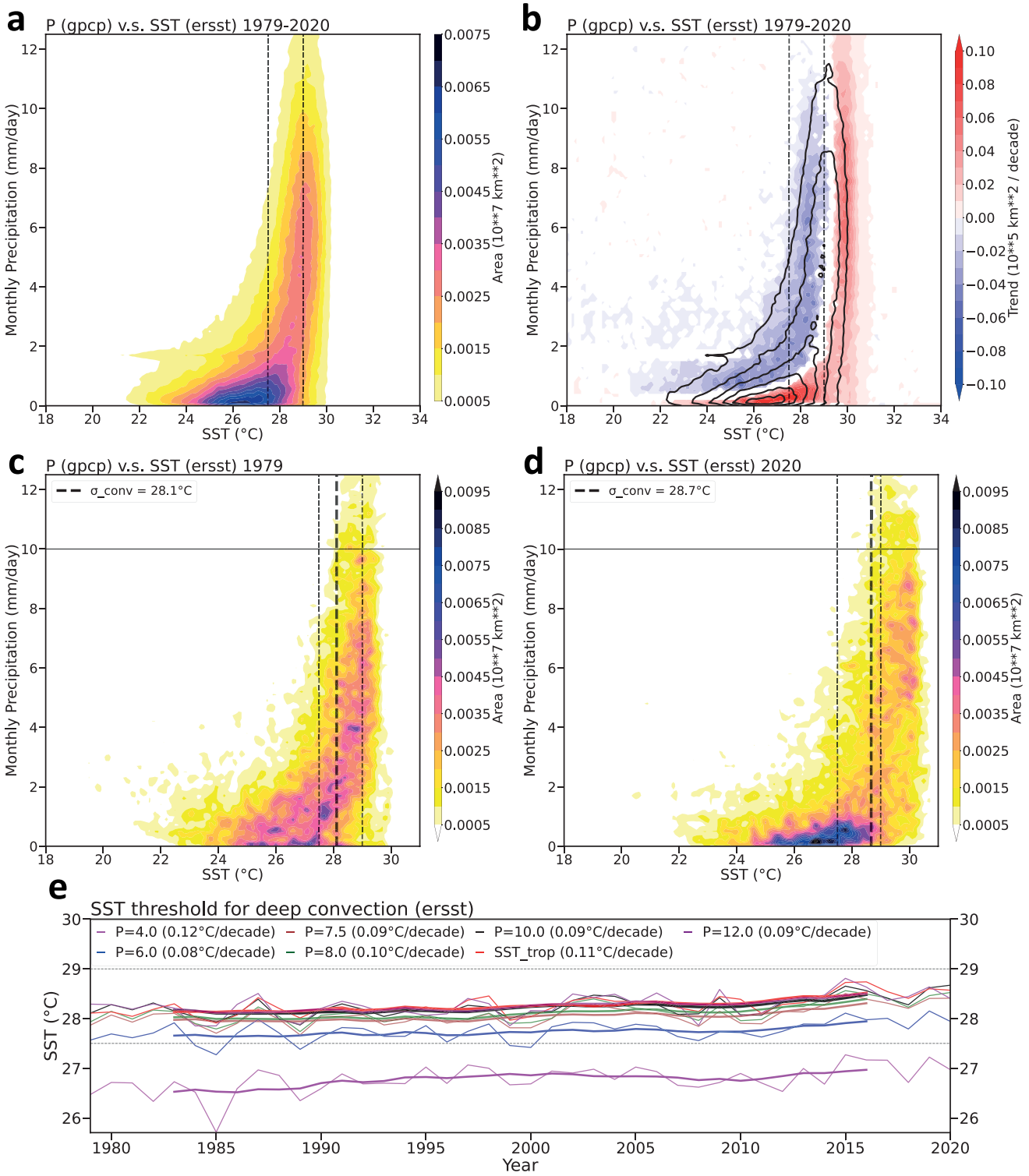

Fig. 1 Increasing SST threshold for IPWP deep convection from 1979–2020. a P-SST JFD averaged over 1979–2020 (shading, 0.05×10^5 km^2 interval). **b** Long-term mean (same as (**a**), contour, 0.1×10^5 km^2 interval) and long-term trend (shading, 0.01×10^5 km^2 interval, only trends being significant at the 90% confidence level are plotted) of the P-SST JFD from 1979–2020. **c**, **d** P-SST JFD (shading, 0.05×10^5 km^2 interval) in 1979 (**c**) and 2020 (**d**). The thin vertical dashed lines in **a**–**d** denote 27.5 °C and 29.0 °C, the common range of IPWP definitions. The thick vertical dashed lines in **c**, **d** denote the estimated σ_{conv} (28.1 °C for 1979, and 28.7 °C for 2020). **e** Time series (thin solid lines) of σ_{conv} (unit: °C) derived from different precipitation criteria and σ_{trop} (unit: °C) over the Indo-Pacific Ocean. The thick solid lines denote 9-year running mean series, which filter out the interannual variability. The linear trends of all series, marked on the figure legend, are statistically significant at the 99.9% confidence level. Results are based on the ERSSTv5 and GPCP precipitation data. The results show that, under greenhouse warming, the observed σ_{conv} of different intensities have been increasing steadily since 1979.

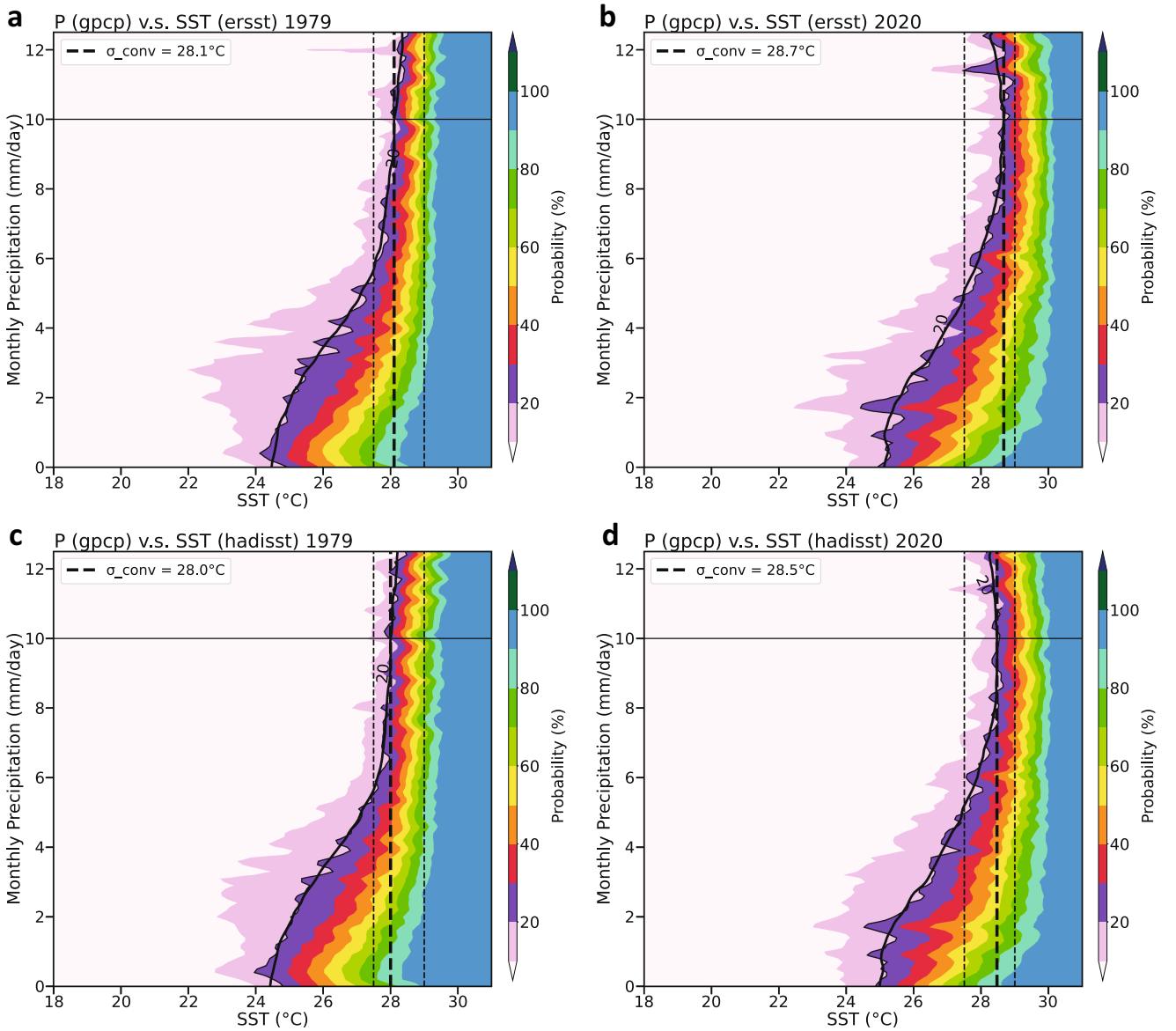

Fig. 2 Changes in the relationship between SST and precipitation over the Indo-Pacific Ocean from 1979 to 2020. a, **b** P-SST JCFD (shading, 10% interval) in 1979 (**a**) and 2020 (**b**), in which the shaded area indicates the probability that a certain precipitation rate occurs below an SST value. Thick solid curves are the 20% contour lines of JCFD smoothed by a 21-point running mean filter. Thin solid lines mark the 10 mm/day precipitation level and the estimated σ_{conv}. The thin vertical dashed lines denote 27.5 °C and 29.0 °C, the common range of IPWP definitions. The thick vertical dashed vertical lines in denote the estimated σ_{conv}. Results are based on ERSSTv5 and GPCP precipitation data. **c**, **d** same as (**a**) and (**b**), except that the SST data are based on the HadISST dataset. The results show the changing relationship between SST and deep convection, with the P-SST JCFD shifting to the right, which indicates an increase in σ_{conv} over the Indo-Pacific Ocean from 1979 to 2020.

Indo-Pacific Ocean, suggesting that the static SST = 28 °C threshold will inevitably become infeasible to characterize convective activities as the bar for deep convection rises in a warmer climate. Hence, the changes in σ_{conv} should be considered in the analyses on the long-term variability of the IPWP features. The increasing σ_{conv} implies that using a time-varied σ_{conv} while studying the long-term change of the IPWP may be more physically rational, in terms that the incentive of studying IPWP change is to understand its impacts on atmospheric deep convection activity.

Different expansion speeds between DCFP and OWP_{28} in the past four decades

Although the increasing trend σ_{conv} is not as large as the local SST warming, it has a great impact on our interpretation of the IPWP expansion analyses. Namely, the expansion speed of the OWP_{28} estimated by the static 28 °C threshold could differ greatly from that of the DCFP defined by the time-varied σ_{conv}. In the following analyses, the DCFP is defined as the ocean enclosed by the σ_{conv} (or σ_{trop}) isotherm, marked as $DCFP_{conv}$ ($DCFP_{trop}$) hereafter, and its area change is compared with that of the OWP_{28} (see Methods section). Because the σ_{conv} is determined from the relationship between precipitation and local SST values, the defined $DCFP_{conv}$ reflects the region where the local SSTs reach the threshold that is favorable to deep convections. Note that although the derivation of σ_{trop} does not involve precipitation, the σ_{trop} also approximates the connection between rainfall and local SST, according to previous studies[20,29].

Based on the ERSSTv5 dataset, we find that, from 1979–2020, while both the OWP_{28} and $DCFP_{conv}$ expanded statistically

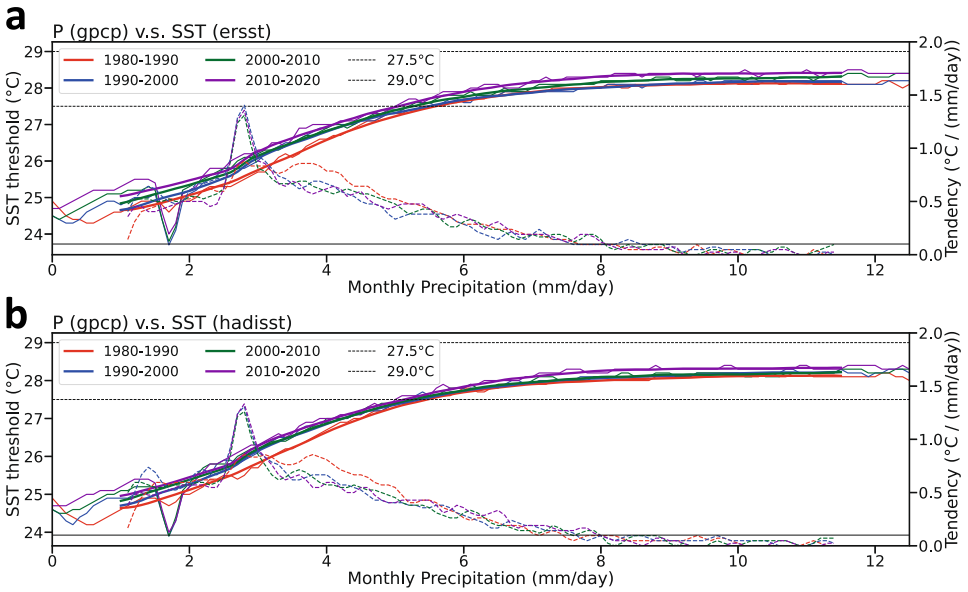

Fig. 3 Relationship between σ_{conv} and precipitation over the Indo-Pacific Ocean in the past four decades. a, **b** Curve (thin solid lines) of σ_{conv} (unit: °C) against precipitation (unit: mm/day) averaged over 1980–1990 (red), 1990–2000 (blue), 2000–2010 (green), and 2010–2020 (purple), based on **a** ERSSTv5 and **b** HadISST datasets. The thick solid lines are the 21-point running mean filtered curve of the thin solid lines, which are equivalent to the 21-point running mean filtered 20% contour lines of JCFD (thick solid lines in Fig. 2). The dashed lines are the slopes (first derivative, unit: °C/(mm/day)) of the 21-point running mean filtered curves. The thin horizontal black dashed lines denote 27.5 °C and 29.0 °C, the common range of IPWP definitions. The results show that while the σ_{conv} slightly shifts upward in the past decades, the relationship between σ_{conv} and precipitation does not exhibit significant changes.

significantly, the increasing trend of the OWP_{28} area (25.02×10^5 km^2/decade, statistically significant at the 99.9% confidence level) is 2.6 times larger than that of the $DCFP_{conv}$ area (9.50×10^5 km^2/decade, statistically significant at the 99.9% confidence level). In comparison, the $DCFP_{trop}$ area does not exhibit significant changes (trend $= -0.31 \times 10^5$ km^2/decade, statistically insignificant). The difference between changes in areas of $DCFP_{conv}$ and $DCFP_{trop}$ results from that between σ_{conv} and σ_{trop}. Namely, the larger σ_{trop} increasing trend causes the smaller and insignificant trend of the $DCFP_{trop}$ area. The constancy of the $DCFP_{trop}$ size compared to the expanding $DCFP_{conv}$ and deep convection area suggests that the SST threshold may not be accurately represented by the tropical mean SST change. It is noted that the OWP_{28} area trend is greater than the expansion trend of the area with a precipitation rate larger than 10 mm/day (hereafter deep convection area) inside the Indo-Pacific Ocean (7.09×10^5 km^2/decade, statistically significant at the 99.9% confidence level; Fig. 4a and Supplementary Fig. 2a). Such difference was suggested to be due to the upper tropospheric warming and insignificant change in SST gradient[18,20,35].

Figures 4b, c visualize the inconsistency between the OWP_{28} and DCFP expansions. In 1979, σ_{conv} and σ_{trop} (28.1 °C) are only 0.1 °C higher than the OWP_{28} definition (28.0 °C), thus the OWP_{28} and DCFP nearly cover the same domain where heavy rainfall is mostly observed (Fig. 4b). However, when the relationship between SST and precipitation changes with climate warming, the difference between σ_{conv} (28.7 °C) and the traditional IPWP definition increases to 0.7 °C in 2020, and the σ_{trop} increases to 28.6 °C. It implies that compared to the past, a warmer ocean surface is required to favor deep convections and heavy rainfall is less likely to be observed with the same SST value in the present day. This is evident in Fig. 4c where a large precipitation rate is mostly observed inside the $DCFP_{conv}$ (blue contour) and the $DCFP_{trop}$ (green contour), but not the region with 28.0 °C < SST < 28.7 °C (the region in between the OWP_{28} and DCFP boundaries). The same conclusion can be drawn based on another independent SST data, the HadISST dataset (Supplementary Fig. 2), as well as based on σ_{conv} derived from different deep convection precipitation criteria (Supplementary Figs. 3 and 4).

The above results illustrate that the increasing SST does not lead to a same increase in the area that fulfills conditions favoring deep convection activity. As a result, the large OWP_{28} area change contradicts the small DCFP area change, implying that the OWP_{28} expansion speed based on the fixed 28 °C threshold is not equivalent to the increase in potential of deep convection occurrence over the Indo-Pacific Ocean. This suggests, in the context of the IPWP inducing climate responses through favoring atmospheric deep convection, that the impacts of IPWP expansion on the global climate may be overestimated if the changing relationship between SST and deep convection under global warming is not considered[9,17,19]. The agreement between the changes in DCFP and deep convection area confirms that the DCFP area change acts as a more reasonable measure for studying the climate effects generated by the Indo-Pacific Ocean warming and suggests the necessity of taking the σ_{conv} variability into account when studying the long-term variability of the IPWP.

Changes in the DCFP size in future climate projections

Although σ_{conv} changes over time, its value generally varied from 27.9 to 28.7 °C in the past four decades, i.e., within the range of traditional definitions of the IPWP (27.5–29.0 °C, Fig. 1e). Thus, its impact on historical IPWP expansion analyses may not be crucial. However, σ_{conv} will further increase, reaching 29.0 °C or higher, in the 21st century based on climate model simulations. In this case, the use of a fixed SST threshold is no longer reasonable for defining the IPWP, as also discussed in previous studies[18]. Based on the future climate projections by 20 Coupled Model Intercomparison Project phase 6 (CMIP6) climate models (see Methods section), which are all able to capture the statistically significant historical increasing trend of σ_{conv} (Fig. 5), we further examine the future changes in the σ_{conv} and $DCFP_{conv}$ size in the 21st century under different emission scenarios.

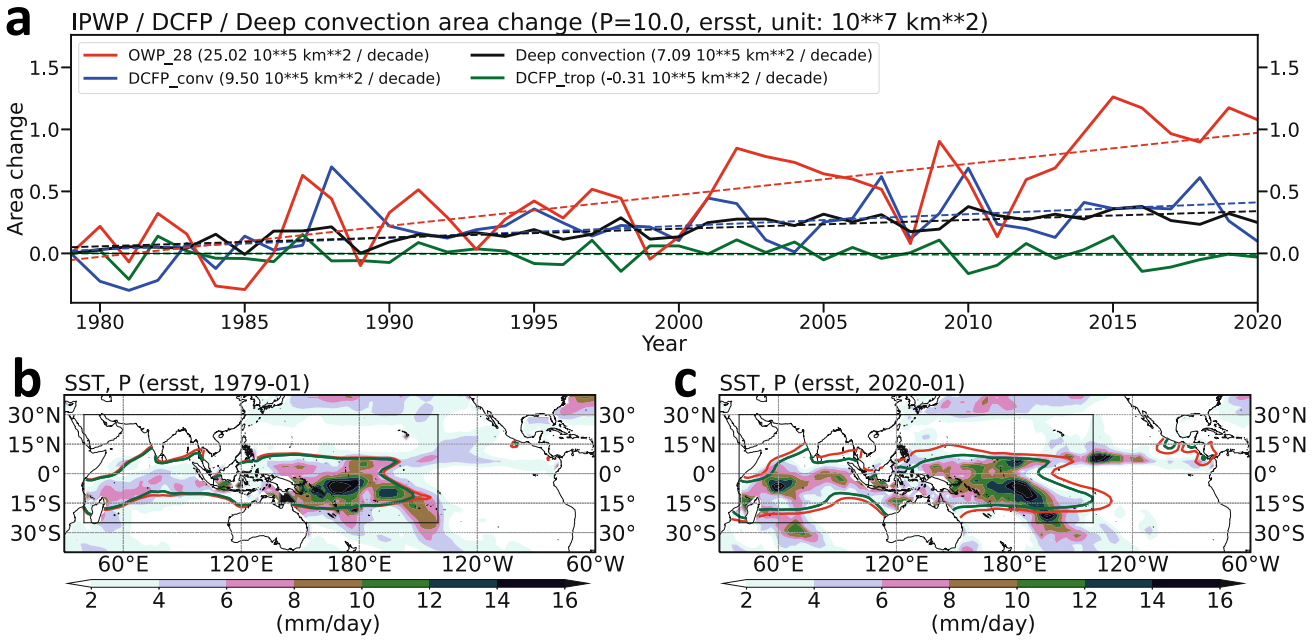

Fig. 4 Changes in the DCFP and OWP_{28} area in the past four decades. a Time series of the area change (unit: 10^7 km^2) of OWP_{28} (red line), $DCFP_{conv}$ (blue line), $DCFP_{trop}$ (green line), and that of the area with monthly precipitation rate larger than 10 mm/day (i.e., deep convection area, black line) inside the Indo-Pacific Ocean (25°S–25°N, 40°E–220°E; black box in **b** and **c**). The linear trends are marked on the figure legend. Trends of all series are statistically significant at the 99.9% confidence level, except that of $DCFP_{trop}$ is statistically insignificant. **b**, **c** Monthly precipitation distribution (shading, 2 mm/day interval) in January 1979 (**b**) and January 2020 (**c**), where the red, blue, and green contours respectively indicate the regions covered by the OWP_{28}, $DCFP_{conv}$ (σ_{conv} = 28.1 °C for 1979 and 28.7 °C for 2020), and $DCFP_{trop}$ (σ_{trop} = 28.1 °C for 1979 and 28.6 °C for 2020). Results are based on the ERSSTv5 and GPCP precipitation data. The results show that as σ_{conv} and σ_{trop} increase, the traditionally defined IPWP may cover a comparatively large region without deep convection. By taking the increase in σ_{conv} into account, the expansion speed of DCFP is ~2.6 times slower than that of IPWP, while the $DCFP_{trop}$ size does not exhibit a statistically significant change.

We first evaluate the ability of the 20 CMIP6 models' ability to simulate the historical changes in the relationship between precipitation and SST. All the models could reproduce the horizontal rightward shift of the P-SST JFD from 1979–2014 in their historical runs. As shown in Fig. 5a, the ensemble P-SST JFD has a similar pattern to that obtained from observed data (Fig. 1a), in terms that large precipitation is more likely to occur when SST is in between 27.5 °C and 30.0 °C. The ensemble simulated P-SST JFD exhibits a long-term rightward shifting trend (Fig. 5b), which is consistent with Fig. 1b. The model simulated σ_{conv} increases together with the rightward shift of P-SST JFD. All the 20 models could capture the historical increasing σ_{conv} trend, with trend values ranging from 0.09 to 0.24 °C/decade. However, the simulated ensemble σ_{conv} trend (0.15 °C/decade) overestimates the observed value (0.07 °C/decade based on ERSSTv5) (Fig. 5c and Table 1). Similarly, the model simulated historical σ_{trop} trend, which shows very similar values (ranging from 0.09 to 0.23 °C/decade with an ensemble value of 0.15 °C/decade) to that of σ_{conv}, is much higher than observation (0.09 °C/decade based on ERSSTv5) (Fig. 5c and Supplementary Table 1). However, there are underestimations of $DCFP_{conv}$ changes, while the ensemble changes in the simulated OWP_{28}, $DCFP_{trop}$ size and deep convection area are relatively close to the observations. Most models (15 out of 20) successfully simulated the increasing trend of the $DCFP_{conv}$ area from 1979 to 2014, but with magnitudes smaller than the observed values and only two (ACCESS-CM2 and CMCC-CM2-SR5) of them gives statistically significant trends at the 99.9% confidence level (Table 2). Meanwhile, 19 models could reproduce the insignificant $DCFP_{trop}$ area trend, except one (MIROC6) gives an statistically insignificant decreasing trend (Supplementary Table 2). It is interesting to note that all the CMIP6 models are unable to reproduce the observed difference between σ_{conv} and σ_{trop} (i.e., the difference between σ_{conv} and tropical mean SST changes). Also, smaller simulated historical $DCFP_{conv}$ expansion rates, compared to the observation, are found in all CMIP6 models (Table 1); and the models overall overestimate the long-term trends of σ_{conv} (Table 2). This may be due to the systematic positive bias of the SST change simulation (Supplementary Table 1). Given that σ_{conv} change is approximately the same as the tropical mean SST increase[20] (Fig. 1e), the positive bias of SST change may lead to the overestimation of σ_{conv} trend and underestimation of $DCFP_{conv}$ expansion rate in model simulations. These may be the reasons for the underestimation of the historical $DCFP_{conv}$ expansion by the CMIP6 models. Based on the evaluation results, 5 models that simulated the $DCFP_{conv}$ area trend mostly consistent with observations are selected as the best models for further investigation of future projections. According to Table 2, the five best models are ACCESS-CM2, CAS-ESM2-0, CESM2-WACCM, CMCC-CM2-SR5, and INM-CM5-0, of which the $DCFP_{conv}$ area trends are 4.23, 3.13, 4.24, 5.74, and 2.74×10^5 km^2/decade, respectively.

As the troposphere continues warming with greenhouse gas concentration increases, the current relationship between SST and convection intensity will further change in the future[18]. The best CMIP6 models projected a long-term rightward shift of the P-SST JFD from 2015–2100, with a larger shift under higher emission scenarios (Fig. 6), indicating the greatest increase in σ_{conv} under the SSP5-8.5 scenario over the Indo-Pacific region. Figure 7a–b give the time series of model-simulated σ_{conv} and σ_{trop} from 1979–2100, revealing similar long-term changes in both σ_{conv} and σ_{trop}, consistent with that in historical runs. Specifically, under the SSP1-2.6 scenario, where the anthropogenic emission peaks by the mid-21st century and the radiative forcing level returns to 2.6 W m^{-2} by 2100, σ_{conv} (σ_{trop}) will first have a steeper increase followed by a relatively constant stage and reach 29.4 °C (29.3 °C) by the end of the 21st century, with their linear trends of 0.09 °C/

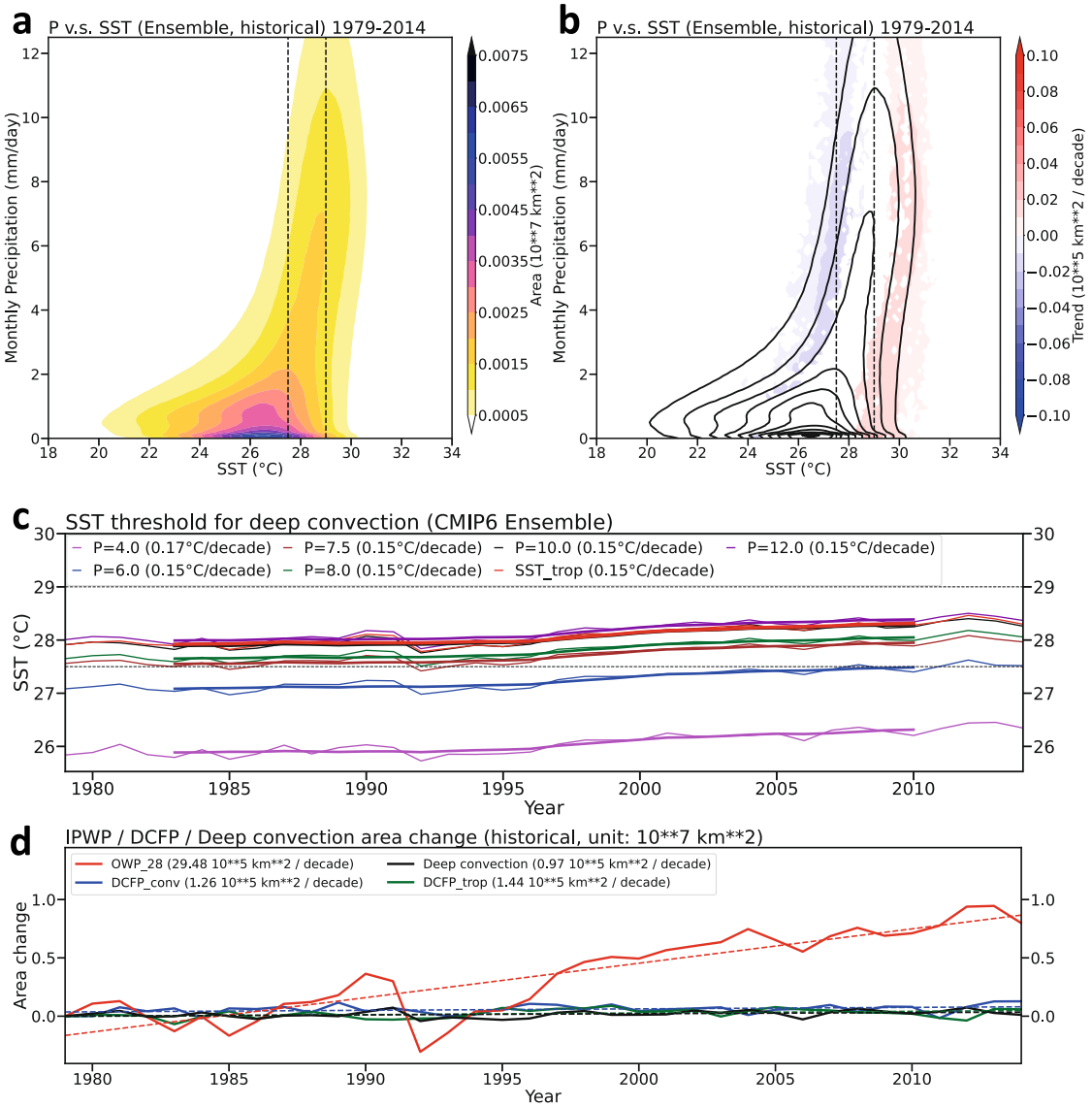

Fig. 5 Historical changes in σ_{conv} and the area of OWP_{28} and DCFP simulated by 20 CMIP6 models. a–d respectively same as Figs. 1a, b, e and 4a, except based on the ensemble historical simulations of 20 CMIP6 models from 1979–2014. The linear trends of all series in **c**, marked on the figure legend, are statistically significant at the 99.9% confidence level. In **d**, the linear trend of the OWP_{28} area is statistically significant at the 99.9% confidence level but those of the other series are insignificant. The results show that the increase in σ_{conv} and the inconsistent expansion speed between OWP_{28} and DCFP are also captured by current climate models. Note the relatively smaller σ_{conv} of the same precipitation level compared to observation, which may be a result of systematic model bias of precipitation simulation.

decade (statistically significant at the 99.9% confidence level) from 2015–2100. Under the stabilized scenario (SSP2-4.5), with a comparatively larger emission and the total radiative forcing is stabilized before 2100, σ_{conv} (σ_{trop}) increases steadily at 0.20 (0.21) °C/decade (statistically significant at the 99.9% confidence level). Both σ_{conv} and σ_{trop} exceeds 29 °C in the second half of the 21st century (after 2040). Under the higher emission scenario (SSP5-8.5), σ_{conv} (σ_{trop}) rises more rapidly, with their long-term linear trends reaching 0.39 (0.41) °C/decade (statistically significant at the 99.9% confidence level), which means that σ_{conv} (σ_{trop}) increases by nearly 4 °C from 1979 and reaches 31.9 °C (31.9 °C) by 2100. No matter under which scenario, both σ_{conv} and σ_{trop} will reach 29.0 °C by or before 2040 (Fig. 7a, b). The σ_{conv} and σ_{trop} for convection with different precipitation levels grow steadily at similar linear trends under the same emission scenario (Fig. 7), but with trend magnitudes being larger under higher emission scenarios (Supplementary Fig. 5). This implies that simply approximating tropical mean SST change as the SST threshold will still likely be a feasible way under different emission scenarios, according to the model simulations.

As a result of the σ_{conv} and σ_{trop} increases, the difference of the area changes between the OWP_{28} and DCFP further increases by the end of the 21st century, with larger differences under higher emission scenarios. The area of OWP_{28} increases rapidly from 2015–2100 at the rates of 12.6, 25.2, and 39.7×10^5 km^2/decade (statistically significant at the 99.9% confidence level) respectively under the SSP1-2.6, SSP2-4.5, and SSP5-8.5 scenarios (Fig. 8). The projected OWP_{28} expansion is characterized by an eastward extension and meridional expansion of the OWP_{28} boundaries. This results in an OWP_{28} further covering part of the eastern Pacific under the SSP1-2.6 projection and covering the whole tropical Indian Ocean and Pacific Ocean under both the SSP2-4.5 and SSP5-8.5 scenarios by 2100, where deep convection less frequently occurs even in the future projection (Fig. 9), which was

Table 1. Long-term trends of σ_{conv} (unit: °C/decade) in the past and future projected climate change, based on ERSSTv5, HadISST, and 20 CMIP6 models.

Observation/models	1979–2020	1979–2014	2015–2100 (SSP1-2.6)	2015–2100 (SSP2-4.5)	2015–2100 (SSP5-8.5)
ERSSTv5	0.09	0.07	/	/	/
HadISST	0.07	0.04	/	/	/
CMIP6 Ensemble	/	0.15	0.07	0.17	0.36
CMIP6 Best	/	0.13	0.09	0.20	0.39
ACCESS-CM2	**/**	**0.13**	**0.11**	**0.22**	**0.46**
CAMS-CSM1-0	/	0.09	0.03	0.11	0.24
CAS-ESM2-0	**/**	**0.16**	**0.12**	**0.23**	**0.40**
CESM2-WACCM	**/**	**0.13**	**0.09**	**0.22**	**0.46**
CMCC-CM2-SR5	**/**	**0.11**	**0.11**	**0.22**	**0.39**
CMCC-ESM2	/	0.14	0.15	0.24	0.43
EC-Earth3	/	0.24	0.07	0.18	0.41
EC-Earth3-Veg	/	0.16	0.07	0.19	0.42
FGOALS-f3-L	/	0.15	0.04	0.15	0.33
FGOALS-g3	/	0.15	0.00*	0.11	0.27
GFDL-ESM4	/	0.16	0.03	0.13	0.30
INM-CM4-8	/	0.15	0.02	0.11	0.26
INM-CM5-0	**/**	**0.14**	**0.03**	**0.10**	**0.25**
IPSL-CM6A-LR	/	0.22	0.07	0.24	0.51
MIROC6	/	0.16	0.06	0.15	0.31
MPI-ESM1-2-HR	/	0.13	0.02	0.14	0.29
MPI-ESM1-2-LR	/	0.12	0.03	0.13	0.30
MRI-ESM2-0	/	0.10	0.06	0.17	0.35
NESM3	/	0.19	0.05	0.16	0.39
TaiESM1	/	0.19	0.15	0.25	0.44

Bold texts denote the five models that could better capture the historical $DCFP_{conv}$ area trend. All trends are statistically significant at the 99.9% confidence level, except those marked with asterisks.

also reported in a previous study comparing the sizes of OWP_{28} and dynamic warm pool[18]. Thus, it is evident that the OWP_{28} expansion rate based on the constant 28 °C SST threshold does not indicate a change in convection activity supported by the warm ocean surface, and hence does not realistically reflect the influence of IPWP on the global climate system under greenhouse warming.

Comparatively, the model-predicted DCFP expansion is much smaller than that of the OWP_{28} and is more consistent with the change in the deep convection area. Compared to the OWP_{28} area trend, the $DCFP_{conv}$ expansion rate is 12–27 times slower under different emission scenarios. The increasing trends of $DCFP_{conv}$ area are rather insignificant under the SSP1-2.6 (0.46×10^5 km^2/decade) and slow under the SSP2-4.5 (1.45×10^5 km^2/decade, statistically significant at the 99.9% confidence level) scenarios, which are respectively 27 and 17 times smaller than that of the OWP_{28}. Although the $DCFP_{conv}$ area under the SSP5-8.5 has a greater increasing trend (3.24×10^5 km^2/decade, significant at the 99.9% confidence level) from 2015–2100, it is 12 times smaller than the OWP_{28} expansion speed (Fig. 8 and Table 2). By the end of the 21st century, the $DCFP_{conv}$ will remain within the Indian Ocean and western Pacific Ocean, instead of extending to the eastern Pacific Ocean as does the OWP_{28}. Similar to the historical observation (Fig. 4b–c), the smaller trend of the projected $DCFP_{conv}$ area is more consistent with that of the deep convection area (Fig. 9). The projected $DCFP_{trop}$ also shows very similar results. The $DCFP_{trop}$ size remains almost the same under the three emission scenarios, with statistically insignificant trends (Fig. 8 and Supplementary Table 2), and stays within the Indian Ocean and western Pacific Ocean. The difference in area changes of the OWP_{28} and DCFP are also shown in the time series (Supplementary Figs. 6–8) and horizontal plots (Supplementary Figs. 9–11) obtained from other CMIP6 models. Both the projected DCFP region is consistent with the position of the Pacific Walker Circulation upper branch which does not expand along with the OWP_{28} in the future warming climate, despite its weakening trend[28,36] (Supplementary Fig. 12). These results indicate that the expansion of DCFP, which considers the long-term variability of σ_{conv} (or σ_{trop}), has a more reasonable physical basis that estimates the impacts of changing IPWP area on the global climate system via modulating deep convection activity under past and future climate change.

DISCUSSION

The analyses presented here illustrate from the deep convection view that due to the increasing SST threshold for deep convection (σ_{conv}) over the Indo-Pacific Ocean, the traditional IPWP definition (static SST = 28 °C threshold) becomes infeasible to characterize convective activities as the bar for deep convection rises in a warmer climate. We thus propose defining the IPWP and examining its expansion by considering the time-varied σ_{conv}, namely the deep convection favoring pool (DCFP), in the context of climate change. Despite the changing of σ_{conv} under global warming has been noticed in numerous early publications, many latest studies about the IPWP expansion ignored the σ_{conv} change over time, which is not true because the different warming rates between the upper and lower troposphere partly offset the enhanced atmospheric instability caused by sea surface warming[18,20,21,29].

Table 2. Long-term trends of $DCFP_{conv}$ (unit: 10^5 km^2/decade) in the past and future projected climate change, based on ERSSTv5, HadISST, and 20 CMIP6 model simulations.

Observation/models	1979–2020	1979–2014	2015–2100 (SSP1-2.6)	2015–2100 (SSP2-4.5)	2015–2100 (SSP5-8.5)
ERSSTv5	9.50	11.16	/	/	/
HadISST	10.63	13.55	/	/	/
CMIP6 Ensemble	/	1.26*	0.25*	1.08	2.52
CMIP6 Best	/	4.02	0.46*	1.45	3.24
ACCESS-CM2	**/**	**4.23**	**1.21***	**2.29**	**4.18**
CAMS-CSM1-0	/	2.19*	0.77*	1.06*	3.01
CAS-ESM2-0	**/**	**3.13***	**0.68***	**0.98***	**3.60**
CESM2-WACCM	**/**	**4.24***	**−0.36***	**−0.40***	**2.27***
CMCC-CM2-SR5	**/**	**5.74**	**1.73**	**2.41**	**3.57**
CMCC-ESM2	/	2.01*	0.52*	0.92*	1.77*
EC-Earth3	/	0.86*	−0.23*	2.17	4.32
EC-Earth3-Veg	/	−0.20*	0.15*	2.19	3.55
FGOALS-f3-L	/	2.02*	−0.94*	−0.12*	3.05*
FGOALS-g3	/	−1.85*	−0.21*	−0.62*	−0.56*
GFDL-ESM4	/	0.52*	0.21*	0.88*	1.68
INM-CM4-8	/	1.71*	0.17*	0.99*	2.46
INM-CM5-0	**/**	**2.74***	**−0.95***	**2.00**	**2.61**
IPSL-CM6A-LR	/	−0.86*	0.51*	1.55*	3.30
MIROC6	/	−3.34*	0.33*	−0.16*	−0.91*
MPI-ESM1-2-HR	/	1.39*	1.40	0.94*	1.95
MPI-ESM1-2-LR	/	1.54*	−0.27*	1.13*	2.26
MRI-ESM2-0	/	2.13*	0.07*	1.00*	3.50
NESM3	/	0.90*	1.08*	1.07*	2.11
TaiESM1	/	−0.41*	−0.90*	1.25*	2.79

Bold texts denote the five models that could better capture the historical $DCFP_{conv}$ area trend. All trends are statistically significant at the 99.9% confidence level, except those marked with asterisks.

Based on the latest observation and the state-of-the-art climate simulations, our results show that such assumption is approximately valid only in a relatively short period (<10 years), but does not hold on a longer timescale (>40 years). Specifically, σ_{conv} increased by 0.09 °C/decade in the past four decades. The short-term increase (~10 years) in σ_{conv} has unnoticeable effects on the difference between the OWP_{28} and DCFP area (3.3% of the OWP_{28} size), but the difference is nonnegligible if one analyzes the long-term changes of the IPWP (comparing blue and black lines in Fig. 4a) and the difference reaches 12.2% of the OWP_{28} size on a time scale of 40 years, not even mentioning that the σ_{conv} trend could be even larger (0.09–0.39 °C/decade) in the future climate projections. Hence, the OWP_{28} expansion rate calculated based on the static 28 °C IPWP definition overestimates the increase in the warm ocean area that favors deep convection (i.e., DCFP). Consequently, the OWP_{28} expansion trend is 2.6 times larger than that of the $DCFP_{conv}$ from 1979–2020, and the difference enlarges to 12–27 times in future projections of climate models. No matter under which future emission scenarios, in contrast to the fast-expanding OWP_{28}, the $DCFP_{conv}$ will remain within the Indian Ocean and western Pacific Ocean by the end of the 21st century, with a slightly increasing trend of its area. For comparison, the area changes of the $DCFP_{trop}$, which is estimated by assuming the SST threshold changes according to the tropical mean SST variation, is also analyzed and is also shown to stay within the Indian Ocean and western Pacific Ocean both in the past and future. The results are insensitive to models and the definition of σ_{conv}. Besides, CMIP6 model evaluation results show that although most models could reproduce the statistically significant increasing trend of the observed σ_{conv}, all the 20 models overestimate the historical changes in σ_{conv}. Most models failed to capture the slight difference of the linear between σ_{conv} and tropical mean SST change, as shown in observed data. These factors affect the model ability to simulate the realistic DCFP and its long-term variability.

It is worth mentioning that numerous research in early years have already revealed the disagreement between the changes in the OWP_{28} and convection areas. For example, prior research has noted the disagreement between the OWP_{28} and the dynamic warm pool, which was derived from the quantity of CIH and can be regarded as the area with atmospheric updraft. They also show that the dynamic warm pool area did not change much even in the Mid-Holocene and last glacial maximum period when the SST was 2–3 °C lower than the present value, implying that the existence of a constant SST threshold for deep convection does not stand up to simple scrutiny[18]. However, as mentioned at the beginning, many latest relevant research still stick to the traditional IPWP definition[9,17–19]. Thus, a target of this study is to emphasize the necessity of considering the response of the relationship between deep convection and SST to climate change, when studying the long-term variability of the IPWP. Based on the latest observation and model simulations, we estimated and reported the long-term change in the DCFP area by determining the local SST threshold favoring deep convection of each year, which shares the same concept of the IPWP definition.

Another important remark is that local SST is not the only factor influencing the atmospheric convection occurring frequency and intensity. The surface temperature gradient serves as the primary force driving the large-scale atmospheric circulation through producing atmospheric pressure gradient and hence air flow and convergence. For example, the Walker circulation is driven by the

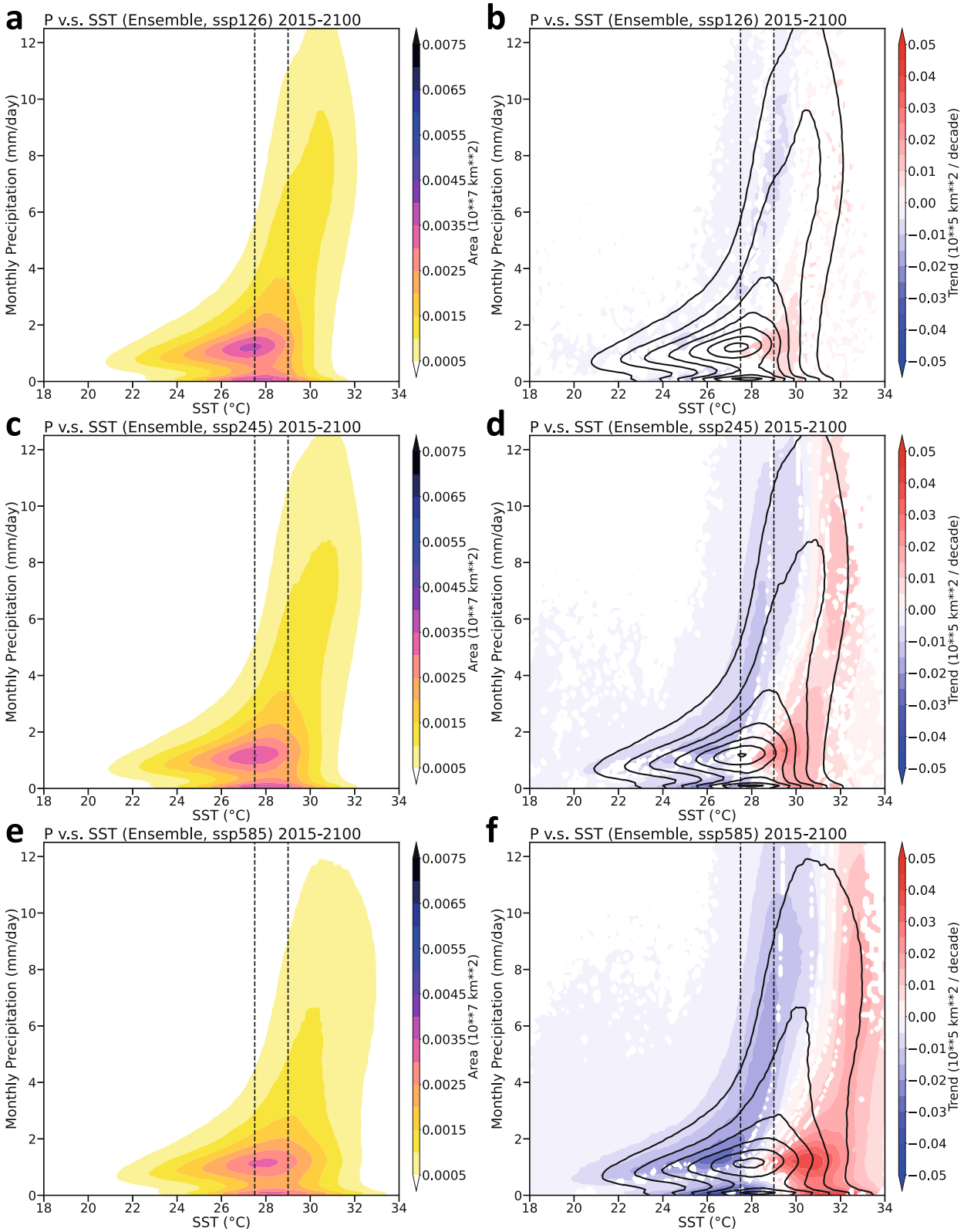

Fig. 6 Changes in the relationship between SST and precipitation over the Indo-Pacific Ocean in climate model simulations. a–c same as Fig. 1a, except based on future climate simulation of the five best CMIP6 models from 2015 to 2100 under the SSP1-2.6 (**a**), SSP 2–4.5 (**b**), and SSP 5-8.5 (**c**) scenarios. **d–f** same as Fig. 1b, except based on future climate simulation of the five best CMIP6 models under the SSP1-2.6 (**d**), SSP 2–4.5 (**e**), and SSP 5-8.5 (**f**) scenarios. The results show that, under future greenhouse warming, the σ_{conv} increases with emission levels, and will no longer be within the range of current IPWP definitions (27.5–29.0 °C).

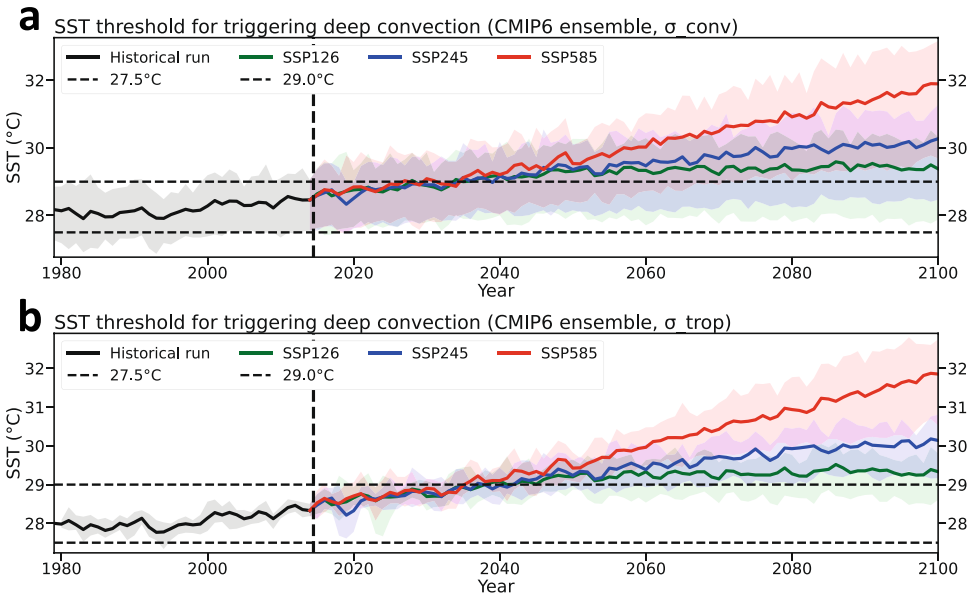

Fig. 7 Variability of SST threshold for deep convection in climate simulations. a, b Time series (unit: °C) of σ_{conv} (**a**) and σ_{trop} (**b**) over the Indo-Pacific Ocean simulated by the five best CMIP6 model under the historical run (black line), SSP1-2.6 (green line), SSP2-4.5 (blue line), and SSP5-8.5 (red line), respectively. Shadings denote the uncertainties of model results. Results show that both the σ_{conv} and σ_{trop} for convection with different precipitation levels grow steadily at similar linear trends under the same emission scenario (see also Table 1 and Supplementary Table 1), but with trend magnitudes being larger under higher emission scenarios.

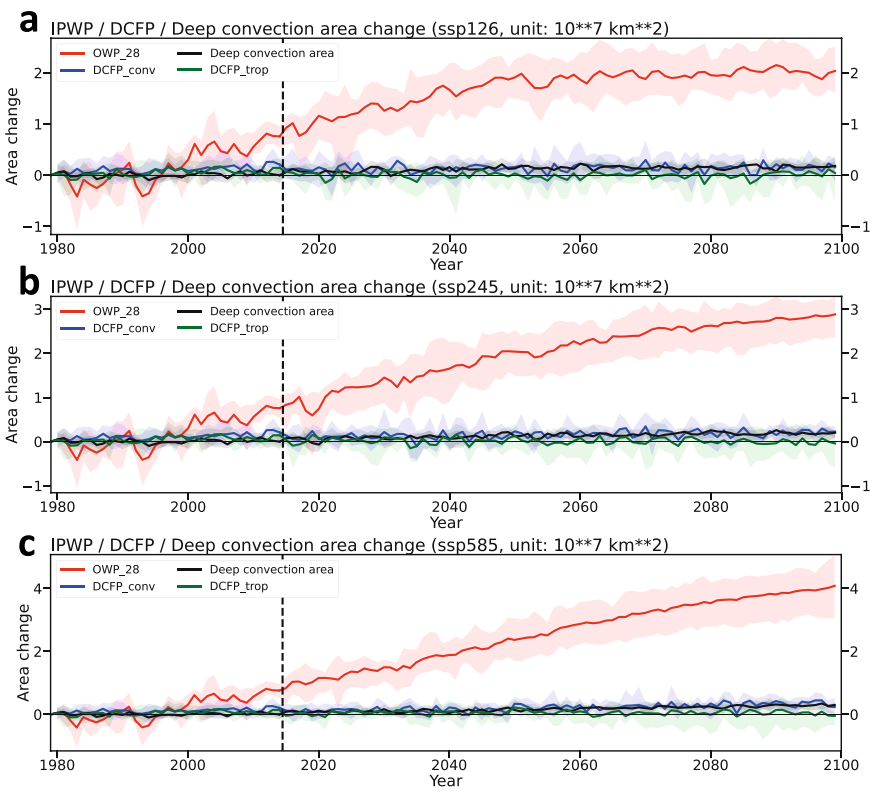

Fig. 8 Long-term change of the DCFP size in future climate projections. a–c Time series of the area change (unit: 10^7 km^2) of the OWP_{28} (red lines), $DCFP_{conv}$ (blue lines), $DCFP_{trop}$ (green lines), and deep convection ($P \geq 10$ mm/day, black lines) inside the Indo-Pacific Ocean under the SSP1-2.6 (**a**), SSP2-4.5 (**b**), and SSP5-8.5 (**c**) scenarios, respectively. Shadings denote the uncertainties of model results. Results are based on the five best CMIP6 models. Results show that the model-predicted $DCFP_{conv}$ expansion is much smaller than that of the OWP_{28} and is more consistent with the change in the deep convection area (see also Table 2).

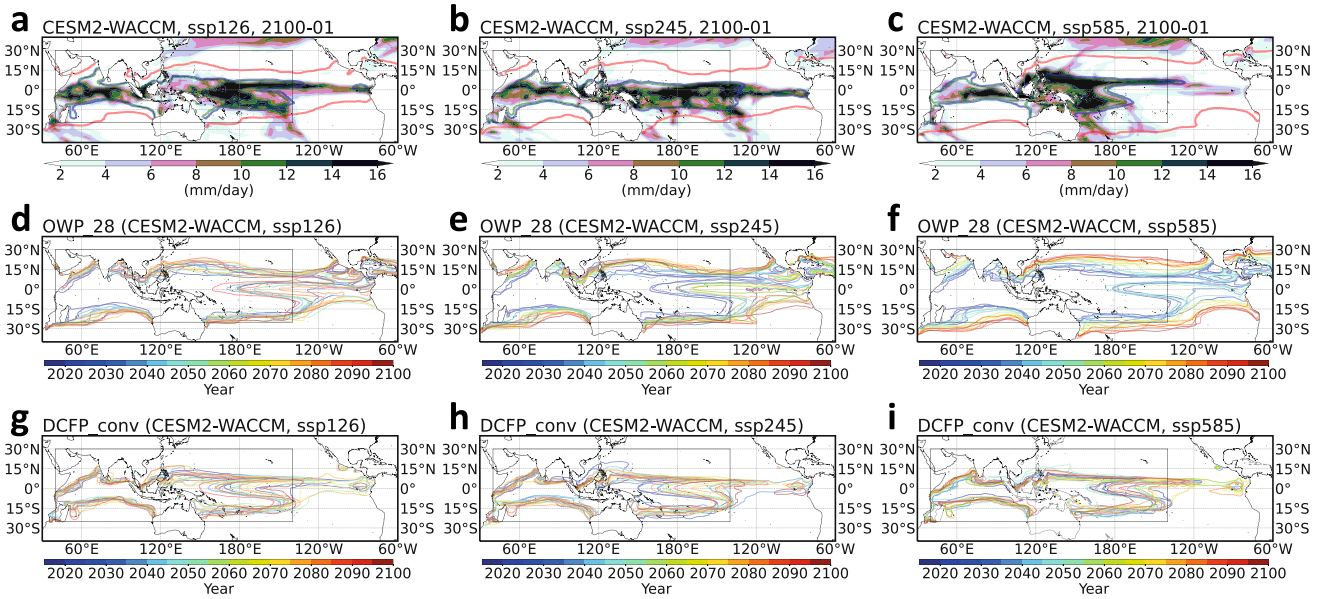

Fig. 9 Model-projected DCFP in the future climate. a–c Monthly precipitation distribution (shading, 2 mm/day interval) in January 2100 under the SSP1-2.6 (**a**), SSP2-4.5 (**b**), and SSP5-8.5 (**c**) scenarios, respectively, where the red, blue and green contours respectively indicate the regions covered by the OWP_{28}, $DCFP_{conv}$, and $DCFP_{trop}$, respectively. **d–i**, Region of the OWP_{28} (**d–f**) and $DCFP_{conv}$ (**g–i**) of every 5 years from 2015–2100 under the SSP1-2.6 (**d**, **g**), SSP2-4.5 (**e**, **h**), and SSP5-8.5 (**f**, **i**), respectively. Results are based on the simulation of CESM2-WACCM, one of the five best models, as an example. The results show that in a future warmer climate, the DCFP will remain within the Indian Ocean and western Pacific Ocean while the IPWP expands to the eastern Pacific, where deep convection is less frequently observed. Results of other models can be found in Supplementary Figs. 9–11.

zonal SST gradient between the Indian Ocean and Pacific Ocean[37–39]. Thus, the DCFP (and also OWP_{28}), which is defined by a local SST threshold, considers solely the effects of local SST on deep convection, without considering other dynamical factors such as SST gradient. Differently, the earlier proposed dynamic warm pool, which is derived based on CIH, can be regarded as defined dynamically by the large-scale coupled ocean–atmosphere system in addition to local SST[18]. The differences of the long-term changes and the physical meaning between the two should be noted according to their definitions.

The IPWP response to greenhouse warming is an important topic of projecting future changes of the global climate system. This study suggests that in a warmer climate, the relationship between SST and deep convection over the Indo-Pacific Ocean has been changing in the past and will be expected to have further changes in the future. Given that the most direct impact of the IPWP on the global climate system is its role in supporting atmospheric deep convection, it is necessary to take the σ_{conv} variability into account when studying how global warming influences the climate system through the IPWP. In this context, we claim that the IPWP expansion estimated based on the fixed σ_{conv} may not reflect the direct impacts of Indo-Pacific warming on the climate system, and the DCFP serves as a more reasonable reference for research about IPWP and climate change. Based on observation and climate model analyses, the DCFP did not and will not expand to a large extent, and will remain within the Indian Ocean and western Pacific Ocean regardless of the anthropogenic emission level. This study, on the basis of the early works[18,20], proposes a more reasonable and feasible way of defining and estimating the IPWP size and its response to climate change, which is important for understanding the impacts of greenhouse warming on the future global climate through the tropical ocean heat source. The σ_{conv} and DCFP data generated in this study can be downloaded from an open repository (see Data availability section).

METHODS

Data

Two monthly SST datasets were analyzed in this study to examine the variability of IPWP and change, including the National Oceanic and Atmospheric Administration (NOAA) Extended Reconstructed Sea Surface Temperature V5 (ERSSTv5) with a $2° \times 2°$ grid[40] and the Hadley Centre Global Sea Ice and SST (HadISST) with a $1° \times 1°$ horizontal resolution[41]. The deep convection activity over the Indo-Pacific Ocean is estimated by the monthly-mean precipitation rate obtained from the Global Precipitation Climatology Project (GPCP) Version 2.3 Combined Precipitation Data Set, which has a $2.5° \times 2.5°$ resolution[42,43].

Apart from observed data, the simulations of 20 the Coupled Model Intercomparison Project phase 6 (CMIP6) models, with data available at the time of analysis, were used in the analyses of the IPWP expansion in future climate conditions, including ACCESS-CM2[44], CAMS-CSM1-0[45], CAS-ESM2-0[46], CESM2-WACCM[47], CMCC-CM2-SR5[48], CMCC-ESM2[49], EC-Earth3[50], EC-Earth3-Veg[50], FGOALS-f3-L[51], FGOALS-g3[52], GFDL-ESM4[53], INM-CM4-8[54], INM-CM5-0[55], IPSL-CM6A-LR[56], MIROC6[57], MPI-ESM1-2-HR[58], MPI-ESM1-2-LR[58], MRI-ESM2-0[59], NESM3[60], and TaiESM1[61] (Table 1). The choices of models depend on their availability of both SST and precipitation data of at the time of analysis. Experiments of the historical run and the future shared socio-economic pathway (SSP) 1–2.6[62], 2–4.5[63], and 5-8.5[64] scenarios were analyzed. Since the GPCP data is available since 1979, the historical analyses presented here start from 1979, and the future climate projections were analyzed over 2015–2100.

Estimation of the changing SST threshold for deep convection (σ_{conv})

To estimate σ_{conv}, we examine the relationship between SST and convection activity over the Indo-Pacific Ocean by making use of the frequency distribution method, or the so-called image histogram approach[65–68], which analyzes the probability frequency distribution (PFD) and the cumulative frequency

distribution (CFD) of a numerical variable (e.g., SST) to determine the probability at which (i.e., the number of grids or the area in which) particular values appear in an image (or a field). The relationship between SST and precipitation can be visualized in the joint frequency distribution (JFD) and the joint cumulative frequency distribution (JCFD) of precipitation versus SST (P-SST JFD and JCFD). The P-SST JFD reflects the joint probability (i.e., area) that certain values of SST and precipitation cover (e.g., Fig. 1a), and the P-SST JCFD indicates the probability (i.e., area) that a certain precipitation rate occurs below an SST value (e.g., Fig. 2a). The image histograms are calculated for each year based on monthly SST and precipitation data inside the Indo-Pacific Ocean region (25°S–25°N, 40°E–220°E), and were applied to further statistical analyses (such as regression analysis and retrieving σ_{conv} etc.).

The detailed procedure for deriving a P-SST JFD is as follows:

(1) Extract monthly observed or model-simulated precipitation and SST data inside the Indo-Pacific Ocean region (25°S–25°N, 40°E–220°E);
(2) For each month, estimate the frequency of each JFD bin by calculating the area of grid points with SST and precipitation values in the range of each bin. The bin widths of SST and P are set to 0.01 °C and 0.1 mm/day, respectively, in this study;
(3) Derive the annual mean P-SST JFDs by averaging the monthly P-SST JFDs of each year;
(4) Plot the estimated frequency value in the form of a two-dimensional histogram, where the x-axis and y-axis indicate the SST and precipitation values, respectively;
(5) Note that, in this study, the frequency value of the JFD is equivalent to the area of grid points, thus the unit of JFD in this paper is presented as km^2;
(6) Also note that one should constrain the total summed frequency of each histogram, which represents the total area, to be equal if the study domain does not change over time.

The calculation of the P-SST JCFD is the same as that of the P-SST JFD, except for step 2. The frequency of each JCFD is estimated by calculating the area of grid points that precipitation values are observed below each SST bin. Again, the bin widths of both SST and P are set to 0.01 °C. The P-SST JCFD reflects the probability that a certain precipitation rate occurs below an SST value, thus the unit of JCFD is presented as %. For instance, in 1979, as shown in Fig. 2a, there is 20% (purple shading of Fig. 2a) of convection with $P = 10$ mm/day occurs when SST is lower than 28.1 °C; in other words, 80% of convection with $P = 10$ mm/day is observed when SST is higher than 28.1 °C in 1979.

The yearly σ_{conv} was derived from the P-SST JCFD (Fig. 2) of each year. Based on the P-SST JCFD, we define $\sigma_{P=P0}$ for convection with a particular precipitation level (P_0) as the minimum SST where more than 80% of the area with $P = P_0$ is observed throughout the year. The choice of 80% is made with the assumption that a small proportion of deep convection is not only triggered purely by warm ocean surface but also induced by other atmospheric systems and dynamic factors, such as tropical waves, tropical cyclones etc. In this study, we take $P_0 = 10$ mm/day as the criterion of deep convection over the Indo-Pacific Ocean, and σ_{conv} is defined as the SST threshold for convection with $P_0 = 10$ mm/day (i.e., $\sigma_{P=10}$). For example, 80% of convection with $P = 10$ mm/day is observed when SST is higher than 28.1 °C in 1979 (Fig. 2a), so the estimated value of $\sigma_{conv} = \sigma_{P=10} = 28.1$ °C in that year. Based on the above approach, σ_{conv} over the Indo-Pacific Ocean has an average value of 28.2 °C, ranging from 27.9 to 28.7 °C during 1979–2020 (Fig. 1e).

The choice of $P = 10$ mm/day as a proxy of deep convection is made based on the variation of $\sigma_{P=P0}$ against P_0. According to early research, atmospheric deep convection is not favored when the SST is lower than a threshold and the continuous rise of SST above the threshold has little effect on increasing the intensity of deep convection[3,69]. As shown in Fig. 3, $\sigma_{P=P0}$ increases gradually with P_0 with a decelerating rate, from ~25 °C at $P_0 = 2$ mm/day to ~28 °C at $P_0 = 12$ mm/day. The increasing rate of $\sigma_{P=P0}$ drops to lower than 0.1 °C/(mm/day) nearly at $P_0 = 8$ mm/day, which implies that the rise of SST does not increase the occurring frequency of P_0 when $P_0 \geq 8$ mm/day. $P_0 = 8$ mm/day is set as the minimum criterion of deep convection. And, since the range of $\sigma_{P=10}$ values (27.9–28.7 °C) is closer to the widely used IPWP definition (28 °C), $P_0 = 10$ mm/day is chosen as the proxy of deep convection in this study. Although the choice of deep convection criterion is partly arbitrary, the conclusions of this manuscript are insensitive to the choice. Analysis results of the σ_{conv} variation and the comparisons between the OWP_{28} and $DCFP_{conv}$ based on different choices of deep convection criteria can be found in Fig. 1 and Supplementary Figs. 3 and 4. It is interesting to point out that, while the extremeness of precipitation may change under the past and future greenhouse warming[30–34], the above reasons for determining the $P_0 = 10$ mm/day as the proxy of deep convection seem not to be affected. According to the CMIP6 model simulations, although the σ_{conv} increases more quickly with higher degree of warming, the changes in the relationship between σ_P against P_0 is insignificant. As shown in Supplementary Figure 13, the increasing rate of $\sigma_{P=P0}$ drops to lower than 0.1 °C/(mm/day) nearly at $P_0 = 9$ mm/day, regardless of emission scenarios. Therefore, we believe the $P_0 = 10$ mm/day deep convection proxy likely will be valid in the future climate status, based on CMIP6 simulations.

In addition, we also define the SST threshold for deep convection based on the changes in the tropical mean SST, which was shown to be a simple but widely used indicator of σ_{conv}[20], for comparisons and mark it as σ_{trop} hereafter. The derivation of σ_{trop} involves three steps:

(1) Calculate the annual mean SST time series averaged over the whole tropical region (20°S–20°N, 360°E);
(2) Adjust the whole annual mean tropical mean SST by adding the difference between σ_{conv} and the tropical mean SST in 1979. This step ensures that both σ_{trop} and σ_{conv} have the same initial value in 1979;
(3) σ_{trop} is defined as the adjusted tropical mean SST time series.

Indo-Pacific Oceanic warm pool area

Following most previous works, the OWP_{28} area is estimated by the total area of the Indo-Pacific Ocean (25°S–25°N, 40°E–220°E) enclosed by the 28 °C SST isotherm[1].

Indo-Pacific deep convection favoring pool area

The DCFP refers to the ocean that fulfils the SST criterion of favoring atmospheric deep convection, which shares the same concept of the traditional IPWP definition except for considering the time-varied σ_{conv}. That is, the DCFP area is defined as the total area of the Indo-Pacific Ocean (25°S–25°N, 40°E–220°E) enclosed by the isotherm of a time-varied SST threshold of deep convection. In this study, two definitions of SST threshold of deep convection were applied: (1) σ_{conv} derived based on $P = 10$ mm/day deep convection criterion, and (2) σ_{trop} derived according to the changes in tropical mean SST. Details of the calculation of σ_{conv} and σ_{trop} are given above.

Linear trend analyses

The statistical significance of all linear trend analyses performed in this study was tested by a two-tailed Student's t-test.

DATA AVAILABILITY

The authors acknowledge the FAIR data policy. Data relevant to the paper can be downloaded from the websites listed below: HadISST provided by the Met Office Hadley Centre at https://www.metoffice.gov.uk/hadobs/hadisst/; ERSSTv5 provided by the NOAA/OAR/ESRL PSL at https://psl.noaa.gov/data/gridded/data.noaa.ersst.v5.html; GPCP provided by the NOAA/OAR/ESRL PSL at https://psl.noaa.gov/data/gridded/data.gpcp.html; CMIP6 model simulation at https://esgf-node.llnl.gov/projects/cmip6/; Data of the estimated σ_{conv} and σ_{trop}, and the corresponding DCFP area in this paper can be found in the repository at https://github.com/jeremychleung/Indo-Pacific-Deep-Convection-Favoring-Pool and https://doi.org/10.5281/zenodo.6977567.

CODE AVAILABILITY

The codes used for analyses in this study are available on request from the authors.

Received: 26 February 2022; Accepted: 4 November 2022;
Published online: 24 November 2022

REFERENCES

1. Weller, E. et al. Human-caused indo-pacific warm pool expansion. *Sci. Adv.* **2**, e1501719 (2016).
2. Yan, X.-H., Ho, C.-R., Zheng, Q. & Klemas, V. Temperature and size variabilities of the western pacific warm pool. *Science* **258**, 1643–1645 (1992).
3. Graham, N. E. & Barnett, T. P. Sea surface temperature, surface wind divergence, and convection over tropical oceans. *Science* **238**, 657–659 (1987).
4. Fasullo, J. & Webster, P. J. Warm pool SST variability in relation to the surface energy balance. *J. Clim.* **12**, 1292–1305 (1999).
5. Williams, A. P. & Funk, C. A westward extension of the warm pool leads to a westward extension of the walker circulation, drying eastern africa. *Clim. Dyn.* **37**, 2417–2435 (2011).
6. Zhan, R., Wang, Y. & Wen, M. The SST gradient between the Southwestern Pacific and the Western Pacific Warm Pool: a new factor controlling the northwestern pacific tropical cyclone genesis frequency. *J. Clim.* **26**, 2408–2415 (2013).
7. Benestad, R. E. On Tropical cyclone frequency and the warm pool area. *Nat. Hazards Earth Syst. Sci.* **9**, 635–645 (2009).
8. Zhang, B. et al. Changes of tropical cyclone activity in a warming world are sensitive to sea surface temperature environment. *Environ. Res. Lett.* **14**, 124052 (2019).
9. Roxy, M. K. et al. Twofold epansion of the Indo-Pacific Warm Pool Warps the MJO life cycle. *Nature* **575**, 647–651 (2019).
10. Lee, S.-K. et al. Pacific origin of the abrupt increase in Indian ocean heat content during the warming hiatus. *Nat. Geosci.* **8**, 445–449 (2015).
11. Rao, S. A. et al. Why is indian ocean warming consistently? *Clim. Change* **110**, 709–719 (2012).
12. Annamalai, H., Hafner, J., Sooraj, K. P. & Pillai, P. Global warming shifts the monsoon circulation, Drying South Asia. *J. Clim.* **26**, 2701–2718 (2013).
13. Hoerling, M., Hurrell, J., Eischeid, J. & Phillips, A. Detection and attribution of twentieth-century northern and southern African rainfall change. *J. Clim.* **19**, 3989–4008 (2006).
14. Ratna, S. B. et al. Moisture variability over the Indo-Pacific region and its influence on the Indian summer monsoon rainfall. *Clim. Dyn.* **46**, 949–965 (2016).
15. Hoerling, M. & Kumar, A. The perfect ocean for drought. *Science* **299**, 691–694 (2003).
16. Zhou, T. et al. Why the Western Pacific subtropical high has extended westward since the late 1970s. *J. Clim.* **22**, 2199–2215 (2009).
17. Park, I.-H., Yeh, S.-W., Min, S.-K. & Son, S.-W. Emergent constraints on future expansion of the Indo-Pacific warm pool. *Geophys. Res. Lett.* **49**, e2021GL097343 (2022).
18. Hoyos, C. D. & Webster, P. J. Evolution and modulation of tropical heating from the last glacial maximum through the twenty-first century. *Clim. Dyn.* **38**, 1501–1519 (2012).
19. Bai, W., Liu, H., Lin, P., Hu, S. & Wang, F. Indo-Pacific warm pool present warming attribution and future projection constraint. *Environ. Res. Lett.* **17**, 54026 (2022).
20. Johnson, N. C. & Xie, S.-P. Changes in the sea surface temperature threshold for tropical convection. *Nat. Geosci.* **3**, 842–845 (2010).
21. Evans, J. L. & Webster, C. C. A variable sea surface temperature threshold for tropical convection. *Aust. Meteorol. Oceanogr. J.* **64**, S1–S8 (2014).
22. Yun, K.-S. et al. Increasing ENSO–rainfall variability due to changes in future tropical temperature–rainfall relationship. *Commun. Earth Environ.* **2**, 43 (2021).
23. Ceppi, P. & Gregory, J. M. Relationship of tropospheric stability to climate sensitivity and earth's observed radiation budget. *Proc. Natl Acad. Sci. USA* **114**, 13126 LP–13113131 (2017).
24. Williams, I. N. & Pierrehumbert, R. T. Observational evidence against strongly stabilizing tropical cloud feedbacks. *Geophys. Res. Lett.* **44**, 1503–1510 (2017).
25. Williams, I. N., Pierrehumbert, R. T. & Huber, M. Global warming, convective threshold and false thermostats. *Geophys. Res. Lett.* **36**, L21805 (2009).
26. Masson-Delmotte, V. et al. *IPCC, 2021: Climate Change 2021: The Physical Science Basis. Contribution of Working Group I to the Sixth Assessment Report of the Intergovernmental Panel on Climate Change*. (Cambridge University Press, 2021).
27. Brown, J. N., Langlais, C., & Sen Gupta, A. Projected sea surface temperature changes in the equatorial pacific relative to the warm pool edge. *Deep Sea Res. Part II Top. Stud. Oceanogr.* **113**, 47–58 (2015).
28. Wu, M. et al. A very likely weakening of pacific walker circulation in constrained near-future projections. *Nat. Commun.* **12**, 6502 (2021).
29. Hu, Z.-Z. et al. Does vertical temperature gradient of the atmosphere matter for El Niño development? *Clim. Dyn.* **48**, 1413–1429 (2017).
30. Donat, M. G., Lowry, A. L., Alexander, L. V., O'Gorman, P. A. & Maher, N. More extreme precipitation in the world's dry and wet regions. *Nat. Clim. Chang.* **6**, 508–513 (2016).
31. Zhang, W. & Zhou, T. Significant increases in extreme precipitation and the associations with global warming over the global land monsoon regions. *J. Clim.* **32**, 8465–8488 (2019).
32. Myhre, G. et al. Frequency of extreme precipitation increases extensively with event rareness under global warming. *Sci. Rep.* **9**, 16063 (2019).
33. Pendergrass, A. G., Lehner, F., Sanderson, B. M. & Xu, Y. Does extreme precipitation intensity depend on the emissions scenario? *Geophys. Res. Lett.* **42**, 8767–8774 (2015).
34. Asadieh, B. & Krakauer, N. Y. Global trends in extreme precipitation: climate models versus observations. *Hydrol. Earth Syst. Sci.* **19**, 877–891 (2015).
35. Lindzen, R. S. & Nigam, S. On the Role of sea surface temperature gradients in forcing low-level winds and convergence in the tropics. *J. Atmos. Sci.* **44**, 2418–2436 (1987).
36. Vecchi, G. A. et al. Weakening of tropical pacific atmospheric circulation due to anthropogenic forcing. *Nature* **441**, 73–76 (2006).
37. Bjerkens, J. Atmospheric teleconnections from the equatorial Pacific. *Mon. Weather Rev.* **97**, 163–172 (1969).
38. Gill, A. E. Some simple solutions for heat-induced tropical circulation. *Q. J. R. Meteorol. Soc.* **106**, 447–462 (1980).
39. Chung, E.-S. et al. Reconciling opposing Walker circulation trends in observations and model projections. *Nat. Clim. Chang.* **9**, 405–412 (2019).
40. Huang, B. et al. Extended reconstructed sea surface temperature, version 5 (ERSSTv5): upgrades, validations, and intercomparisons. *J. Clim.* **30**, 8179–8205 (2017).
41. Rayner, N. A. et al. Global analyses of sea surface temperature, sea ice, and night marine air temperature since the late nineteenth century. *J. Geophys. Res. Atmos.* **108** (2003).
42. Adler, R. F. et al. The version-2 Global Precipitation Climatology Project (GPCP) monthly precipitation analysis (1979–Present). *J. Hydrometeorol.* **4**, 1147–1167 (2003).
43. Huffman, G. J. et al. The Global Precipitation Climatology Project (GPCP) combined precipitation dataset. *Bull. Am. Meteorol. Soc.* **78**, 5–20 (1997).
44. Mackallah, C. et al. ACCESS datasets for CMIP6: methodology and idealised experiments. *J. South. Hemisphere Earth Syst. Sci.* **72**, 93–116 (2022).
45. Rong, X.-Y. et al. Introduction of CAMS-CSM model and its participation in CMIP6. *Adv. Clim. Change Res.* **15**, 540–544 (2019).
46. Zhang, H. et al. Description and climate simulation performance of CAS-ESM version 2. *J. Adv. Model. Earth Syst.* **12**, e2020MS002210 (2020).
47. Danabasoglu, G. NCAR CESM2-WACCM model output prepared for CMIP6 CMIP. https://doi.org/10.22033/ESGF/CMIP6.10024 (2019).
48. Cherchi, A. et al. Global mean climate and main patterns of variability in the CMCC-CM2 coupled model. *J. Adv. Model. Earth Syst.* **11**, 185–209 (2019).
49. Lovato, T. et al. CMIP6 simulations with the CMCC earth system model (CMCC-ESM2). *J. Adv. Model. Earth Syst.* **14**, e2021MS002814 (2022).
50. Döscher, R. et al. The EC-Earth3 earth system model for the coupled model intercomparison project 6. *Geosci. Model Dev.* **15**, 2973–3020 (2022).
51. Zhao, S. et al. Datasets for the CMIP6 Scenario Model Intercomparison Project (ScenarioMIP) simulations with the coupled model CAS FGOALS-f3-L. *Adv. Atmos. Sci.* **38**, 329–339 (2021).
52. Li, L. et al. The flexible global ocean-atmosphere-land system model grid-point version 3 (FGOALS-g3): description and evaluation. *J. Adv. Model. Earth Syst.* **12**, e2019MS002012 (2020).
53. Dunne, J. P. et al. The GFDL earth system model version 4.1 (GFDL-ESM 4.1): overall coupled model description and simulation characteristics. *J. Adv. Model. Earth Syst.* **12**, e2019MS002015 (2020).
54. Volodin, E. et al. *INM INM-CM4-8 model output prepared for CMIP6 CMIP*. https://doi.org/10.22033/ESGF/CMIP6.1422 (2019).

55. Volodin, E. et al. *INM INM-CM5-0 model output prepared for CMIP6 CMIP*. https://doi.org/10.22033/ESGF/CMIP6.1423 (2019).
56. Boucher, O. et al. Presentation and evaluation of the IPSL-CM6A-LR climate model. *J. Adv. Model. Earth Syst.* **12**, e2019MS002010 (2020).
57. Tatebe, H. et al. Description and basic evaluation of simulated mean state, internal variability, and climate sensitivity in MIROC6. *Geosci. Model Dev.* **12**, 2727–2765 (2019).
58. Müller, W. A. et al. A Higher-resolution Version of the Max Planck Institute Earth System Model (MPI-ESM1.2-HR). *J. Adv. Model. Earth Syst.* **10**, 1383–1413 (2018).
59. & Yukimoto, S. et al. The meteorological research institute earth system model version 2.0, MRI-ESM2.0: description and basic evaluation of the physical component*J. Meteorol. Soc. Japan. Ser. II* **97**, 931–965 (2019).
60. Cao, J. et al. NUIST ESM v3 data submission to CMIP6. *Adv. Atmos. Sci.* **38**, 268–284 (2021).
61. Wang, Y.-C. et al. Performance of the Taiwan earth system model in simulating climate variability compared with observations and CMIP6 model simulations. *J. Adv. Model. Earth Syst.* **13**, e2020MS002353 (2021).
62. Meinshausen, M. & Nicholls, Z. R. J. *UoM-IMAGE-ssp126-1-2-1 GHG Concentrations*. https://doi.org/10.22033/ESGF/input4MIPs.9865 (2018).
63. Meinshausen, M. & Nicholls, Z. R. J. *UoM-MESSAGE-GLOBIOM-ssp245-1-2-1 GHG Concentrations*. https://doi.org/10.22033/ESGF/input4MIPs.9866 (2018).
64. Meinshausen, M. & Nicholls, Z. R. J. *UoM-REMIND-MAGPIE-ssp585-1-2-1 GHG Concentrations*. https://doi.org/10.22033/ESGF/input4MIPs.9868 (2018).
65. Chen, J., Carlson, B. E. & Del Genio, A. D. Evidence for strengthening of the tropical general circulation in the 1990s. *Science* **295**, 838–841 (2002).
66. Motoyoshi, I., Nishida, S., Sharan, L. & Adelson, E. H. Image statistics and the perception of surface qualities. *Nature* **447**, 206–209 (2007).
67. Kravchenko, A. N. et al. Microbial spatial footprint as a driver of soil carbon stabilization. *Nat. Commun.* **10**, 3121 (2019).
68. Tsurusaki, Y. et al. De Novo SOX11 mutations cause coffin–siris syndrome. *Nat. Commun.* **5**, 4011 (2014).
69. Zhang, C. Large-scale variability of atmospheric deep convection in relation to sea surface temperature in the tropics. *J. Clim.* **6**, 1898–1913 (1993).

ACKNOWLEDGEMENTS

This work is supported by the Guangdong Province Introduction of Innovative R&D Team Project China (2019ZT08G669), the Southern Marine Science and Engineering Guangdong Laboratory (Zhuhai), the Guangdong Basic and Applied Basic Research Foundation (2020A1515110275), the National Natural Science Foundation of China (41776031).

AUTHOR CONTRIBUTIONS

J.C.H.L.: methodology, formal analysis, data curation, writing—original draft, writing—review and editing, and visualization; B.Z.: conceptualization, supervision, methodology, writing—review and editing, and funding acquisition; Q.G.: formal analysis, data curation, writing—review and editing; L.W., W.Q., and Z.Z.H.: writing—review and editing. All authors reviewed the manuscript.

COMPETING INTERESTS

The authors declare no competing interests.

ADDITIONAL INFORMATION

Supplementary information The online version contains supplementary material available at https://doi.org/10.1038/s41612-022-00315-w.

Correspondence and requests for materials should be addressed to Banglin Zhang.

Reprints and permission information is available at http://www.nature.com/reprints

Publisher's note Springer Nature remains neutral with regard to jurisdictional claims in published maps and institutional affiliations.